Supplemental Materials

Probabilistic human health risk assessment of perfluorooctane sulfonate (PFOS) by integrating *in vitro*, *in vivo* toxicity, and human epidemiological studies using a Bayesian-based dose-response assessment coupled with physiologically based pharmacokinetic (PBPK) modeling approach

Wei-Chun Chou, Zhoumeng Lin*

[1] Institute of Computational Comparative Medicine (ICCM), Department of Anatomy and Physiology, College of Veterinary Medicine, Kansas State University, Manhattan, KS 66506, United States

Wei-Chun Chou: weichunc@vet.k-state.edu; Zhoumeng Lin: zhoumeng@ksu.edu

* Corresponding author. Email: zhoumeng@ksu.edu; Phone: +1-785-532-4087; Fax: +1-785-532-4953; Address: 1800 Denison Avenue, P200 Mosier Hall, Institute of Computational Comparative Medicine (ICCM), Department of Anatomy and Physiology, College of Veterinary Medicine, Kansas State University, Manhattan, KS 66506, United States

Table of Content

1. Dose-response data sets

In this study, we collected dose-response data sets from human epidemiological studies, animal *in vivo* toxicity studies and ToxCast *in vitro* assays for a comprehensive dose-response evaluation. The datasets consisted of 34 studies and 7 endpoints: increased serum cholesterol, increased liver weight, PPAR activation, neurotoxicity, immunotoxicity, endocrine disruption and cellular responses (including cytotoxicity, mitochondria, oxidative stress, DNA binding and cell cycle). The datasets are listed in Table 1 and Table 2 of the manuscript.

1.1 Human epidemiological studies

1.1.1 Mode of action (MOA) considerations for human studies

According to the comprehensive literature review by EFSA (EFSA, 2018), numerous human studies have investigated potential association between PFOS or PFOA exposure and serum cholesterol levels. Most of them show significant positive associations between PFOS and/or PFOA and total cholesterol (Eriksen et al., 2013; Fitz-Simon et al., 2013; Frisbee et al., 2010; Geiger et al., 2014; Skuladottir et al., 2015; Starling et al., 2014; Steenland et al., 2009; Yu et al., 2005). For PFOS, only one of these studies shows clear null results (Lin et al., 2011). Based on these human studies, EFSA concludes that it's likely there is a causal association between PFOS and increase of serum cholesterol. However, the exact mechanism of how PFOS increases human serum cholesterol levels remains unclear. Based on the latest EPA report (U.S. EPA, 2016), the possible MOA is that high-density lipoproteins (HDLs) bind cholesterol from other serum lipoprotein complexes and transport it to the liver for degradation and conversion to bile salts (Montgomery et al. 1990). Competition between PFOS and bile salts for biliary transport could result in impeded removal of HDL lipids from serum and increase both HDL cholesterol and total cholesterol. In addition, HDLs have the highest ratio of proteins to lipids (50:50) among the serum

lipoprotein complexes (Montgomery et al. 1990). Binding of PFOS to HDL protein could impede the HDL interaction with liver tissue receptors resulting in increased serum levels of HDL. However, the inverse association between cholesterol and serum PFOS concentration was observed in rodents (Elcombe et al., 2012; Minata et al., 2010; Wang et al., 2013). The differences of susceptibility between primates and rodents on the activation of PPARa might be one of reasons to account for this species-specific effect. Additional studies are needed to elucidate the mechanisms of how PFOS changes serum cholesterol concentrations in different species.

1.1.2 Selected critical human epidemiological studies

Numerous epidemiologic studies have evaluated the potential association between serum lipid status and plasma PFOS concentrations, and they have reported a significant association between PFOS exposure and the increase in total serum cholesterol level in the general population (Table 1). Four cohort studies were included in our dose-response analyses with different human populations, including the U.S. NHANES (National Health and Nutrition Examination Survey) volunteers (Nelson et al., 2010), the U.S. C8 Health Project participants (Steenland et al. 2009), Danish population (Eriksen et al., 2013), and Inuit population (Château-Degat et al., 2010)

- **U.S. population:** Steenland et al. (2009) examined the levels of serum PFOS, PFOA, and lipids among 46,294 residents, ≥18 years old, participating in the C8 Health Project. The mean serum PFOS levels were determined to be 0.022 μg/mL with a range of 0.00025 – 0.7592 μg/mL. The lipid outcomes including total cholesterol, HDL cholesterol, LDL cholesterol, and triglycerides were determined to investigate the potential association between serum PFOA/PFOS levels and the lipid endpoints. In the NHANES study, Nelson et al. (2010) used the 2003–2004 data to analyze PFOS and other perfluorinated chemicals and lipid outcomes (total cholesterol, HDL, non-HDL lipoproteins, and LDL).

Approximately 860 participants (20-80 years old) were included in the analyses with the mean PFOS serum concentration of 0.025 µg/mL (range: 0.0014–0.392 µg/mL). A significant positive association was identified between total serum cholesterol and serum PFOS concentrations.

- **Danish population:** In the Danish cohort (n = 753; 663 males and 90 females), Eriksen et al. (Eriksen et al., 2013) examined the association between plasma PFOS levels and total cholesterol levels in a middle-aged (50-65 years) Danish population. The mean plasma PFOS level was 0.0361 µg/mL. A significant positive association was found between serum PFOS levels and total serum cholesterol levels. In addition, a 4.6 mg/dL (95% CI: 0.8–8.5) higher concentration of total cholesterol was found per interquartile range of plasma PFOS level.
- **Inuit population:** In the Inuit population (n = 723), a cross-sectional epidemiological study was conducted to evaluate the effect of PFOS exposure on blood lipids. The mean PFOS concentration was 18.6 ng/mL (geometric mean) with 95% CI of 17.8 – 19.5 ng/mL. A positive trend was identified between total cholesterol and PFOS exposure, but it was no longer statistically significant after an adjustment for confounders.

1.2. Animal *in vivo* toxicity studies

1.2.1 Mode of action (MOA) considerations for animal studies

Many experimental studies have shown that the liver is the primary target organ for PFOS in animals (Fai Tse et al., 2016; Han et al., 2018; Wan et al., 2016). However, the MOA responsible for the increase of liver weight due to PFOS exposure is not well understood. Based on the EFSA report (EFSA, 2018), one of possible mechanisms of PFOS-induced liver toxicity appears to be the activation of xenobiotic-sensing nuclear receptors such as PPARα, constitutive androstane

receptor (CAR), and pregnane X receptor (PXR) in the liver. The association of the incidence of liver tumor and hepatomegaly with the activation of xenosensor nuclear receptors in rodents has been well established (Lake, 2009). Specifically, the increase in liver weight can result from increased peroxisomal mass and expansion of the smooth endoplasmic reticulum by the activation of PPARα (Vanden Heuvel et al., 2006). The activation of CAR and PXR can also increase liver weight through the production of cytochromes with a consequent increase in cytochromal proteins (Elcombe et al., 2014). In addition, activation of PPARα, CAR, or PXR in rodents may trigger replicative DNA synthesis, resulting in proliferation of hepatocytes, and may decrease apoptosis of hepatocytes, potentially leading to clonal expansion of preneoplastic foci and, ultimately, liver carcinogenesis (Lake, 2018; Shizu et al., 2013). However, the mechanism for the observed liver toxicity in primates might be different from rodents because recent studies have shown relative less susceptibility of primates compared with rodents to peroxisome proliferation (Gonzalez and Shah, 2008). There might be other pathways/mechanisms by which PFOS can interfere with lipid metabolism in the liver in primates. Recently, Xu et al. (Xu et al., 2017) reported that the ERβ knockout mice did not have the adverse effects (hepatocyte vacuolization, hydropic degeneration, changes in levels of cholesterol and bile acids) that were observed in PFOS-exposed wild-type mice, suggesting the PFOS-induced liver toxicity may also involve the ERβ pathway.

1.2.2 Selected critical animal studies

Six animal studies in different species including the mouse, rat and monkey were included in our dose-response analyses (Table 1). These studies consistently show that PFOS exposure is significantly associated with increased absolute/relative liver weight. These studies are described in detail below:

- **Mouse**: Two mouse studies were included in our analyses. Dong and his co-workers

conducted two mouse studies for PFOS exposure published in 2009 (Dong et al., 2009) and 2011 (Dong et al., 2011), respectively. Although the studies aimed to examine PFOS-induced immunotoxicity, the liver weight was also measured and found to be increased significantly. In the first study (Dong et al., 2009), adult male C57BL/6 mice were exposed to PFOS daily via oral gavage for 60 days at the dose of 0, 0.5, 5, 25, 50, or 125 mg/kg/day. Their results showed that liver weight was significantly increased at the groups of ≥5 mg/kg/day in a dose-dependent manner. In the second study (Dong et al., 2011), adult male C57BL/6 mice were exposed to PFOS daily via oral gavage for 60 days at the dose level of 0, 0.5, 5, 25, or 50 mg/kg/day. The results showed that several immune biomarkers were altered in a dose-dependent manner at ≥5 mg/kg/day dose groups, and the liver weight was also significantly increased at doses as low as 25 mg/kg/day.

- **Rat**: Three rat studies were included in our analyses. In the first study, Seacat and his co-workers (Seacat et al., 2003) conducted a 14-week (98-day) study in Sprague-Dawley (SD) rats. Rats were administered PFOS via the diet at concentrations of 0, 0.5, 2, 5, and 20 ppm (i.e., 0, 0.03, 0.13, 0.34, and 1.33 mg/kg in males and 0, 0.04, 0.15, 0.40, and 1.56 mg/kg in females) for 14 weeks (98 days). A thorough necropsy was performed at the end of treatment, and liver samples were collected. Absolute and relative (to body weight) liver weights were increased significantly in the males and males/females, respectively. In the second study (Curran et al., 2008), Sprague-Dawley rats were treated with PFOS at 0, 0.14, 1.33, 3.21 or 6.34 mg/kg/day for 28 days, and the changes in clinical chemistry, hematology, histopathology, tissue residues and other effects were assessed. Tissue residue results showed a dose-dependent increase in most groups and mostly observed in liver. In the third study (Lefebvre et al., 2008), Sprague-Dawley rats were exposed to PFOS via dietary

exposure for 28 days at the doses ranging from 0.14 to 7.58 mg/kg/day and compared with those receiving control diet. The results showed that the body weight was significantly reduced in male and female rats exposed to 50 and 100 mg PFOS/kg diet. Moreover, the liver weight was significantly increased in females exposed to 2 mg/kg diet and in males exposed to 20 mg/kg diet.

- **Monkey**: Only one monkey study was included in our study. Seacat et al. (2002) administered 0, 0.03, 0.15, or 0.75 mg/kg/day of PFOS orally in a capsule by intragastric intubation to cynomolgus monkeys (n=6). PFOS levels were determined in serum and liver tissue. Except for the group of 0.03 mg/kg/day, animals in other groups were exposed to PFOS for 26 weeks (182 days). Liver samples were obtained for hepatic peroxisome proliferation determination and immunohistochemistry. Mean absolute and relative (to body weight) liver weights were increased significantly in the 0.75 mg/kg/day dose group for both males and females.

1.3. ToxCast *in vitro* assays

1.3.1 Mode of action (MOA) considerations for *in vitro* studies

The Toxicity Forecaster (ToxCast) database includes a large amount of high throughput screening datasets of *in vitro* and *in vivo* assays on over 9,000 chemicals. The 24 PFOS-activated *in vitro* assays which may link to PFOS-induced adverse outcomes were selected. The use of these *in vitro* assays was based on the hypothesis that these molecular initiating events (i.e., receptor activation) triggered by PFOS exposure might link cellular perturbations to adverse outcomes. For example, PPAR and ER activation support the MOA of PFOS-induced liver toxicity of PFOS observed in animal studies described previously (Chou et al., 2017; Das et al., 2017; Palmisano et al., 2017). In addition, the cellular responses, such as cytotoxicity, oxidative stress, DNA binding and cell

cycle effects have been reported to link to the PFOS-induced toxicity (Pierozan and Karlsson, 2018). However, more specific mechanisms of each of these *in vitro* endpoints remain to be investigated.

1.3.2 Selected critical ToxCast *in vitro* assays

Twenty-four ToxCast assays were included in our study as shown in Table 2. These assays were designed to evaluate the effects of chemicals (e.g., PFOS) on the activities of human enzymes and transcription factors, including cell-free enzymatic and ligand-binding high-throughput screening assays (labeled with "NVS") (Sipes et al., 2013), cell-based nuclear receptors and transcription factor response element (labeled with "ATG") (Martin et al., 2010), cell-based high-content imaging (labeled with "APR") (Shah et al., 2016) and cell-based protein expression (labeled with "BSK") (Houck et al., 2009). Based on the U.S. EPA report (U.S. EPA, 2016), these *in vitro* dose-response data sets were categorized into six groups by the molecular targets, including PPAR activation, neurotoxicity (*in vitro*), immunotoxicity, endocrine disruptors, and cellular responses (including cytotoxicity, mitochondria, oxidative stress, DNA binding and cell cycle effects). These molecular targets are discussed in detail below:

- **PPAR activation:** Several studies have reported that PFOS can activate the PPAR pathway (Palmer et al., 1998; Shipley et al., 2004; Takacs and Abbott, 2007). In the ToxCast program, PFOS was found to induce DNA expressions of PPAR alpha (PPARα), peroxisome proliferator hormone response elements (PPRE), PPAR gamma (PPARγ), and to antagonize PPARγ receptor (Wambaugh et al., 2013). We included PPARα, PPRE and PPARγ assays in the present dose-response analysis.
- **Neurotoxicity:** Five different neurological receptor families with seven different receptor types in ToxCast cell-based assays were activated by PFOS, including 5-

hydroxytryptamine receptor (5HT) 5a, 6, and 7, adenosine A2a receptor (ADORA2), adrenoceptor alpha 2C (ADRA2C), and beta 1 (ADRB1) (U.S. EPA, 2016). These receptors are involved in the effects of neurotoxicity and were included in our study.

- **Immunotoxicity:** In the ToxCast program, PFOS was found to be able to induce the expression of a variety of genes associated with immunotoxicity, such as chemokine ligand (CXCL) 10, CXCL8, collagen type II alpha (COL3A), interleukin-1 alpha (IL-1α), plasminogen activator (PLA), plasminogen activator urokinase (PLAUR), vascular cell adhesion molecule (VCAM1), and the TNF receptor subfamily gene CD40 (CD40) (U.S. EPA, 2016). Among these genes, VCAM1 and PLAUR have been reported to induce chronic inflammation and vascularization *in vivo* (Kleinstreuer et al., 2013). In this study, we included CXCL10, CXCL8, IL-1α, CD4, PLAUR, and VCAM1 ToxCast *in vitro* assays in the category of immunotoxicity dose-response analysis.
- **Endocrine disruption:** Estrogen and its related receptors have been associated with sexual development and reproductive function and cancer (Makela et al., 1994). Four different estrogen receptor assays, all of which were related to estrogen receptor α (ESR α), were included in our study. In addition, the thyroid hormone receptor α was also included in the category of endocrine disruption dose-response analysis.
- **Cellular response:** Several *in vitro* studies have shown that PFOS exposure can cause multiple cellular responses, including inhibition of DNA synthesis, deficits in cell growth and oxidative stress (Hu and Hu, 2009; Slotkin et al., 2008). These *in vitro* effects might help elucidate the toxic mechanisms of PFOS (Chen et al., 2014; Zeng et al., 2019). Thus, the cellular responses detected in ToxCast program, including cytotoxicity, oxidative stress, DNA binding and cell cycle effects were included in the dose-response analyses.

2. Bayesian hierarchical model

In this study, we proposed a three-stage Bayesian hierarchical model for the dose-response analysis (Fig. S1). In the first level (i.e., the experiment level), our model accounted for the variability within experiment. The variable y_{ij} was denoted as measured response in the study j at the dose level i and was assumed to be distributed normally around the predicted value μ_{ij}.

$$y_{ij} \sim N(\mu_{ij}, \varepsilon) \quad \textbf{S1}$$

The measured response was modeled as a linear function of the dose: $y_{ij} = \mu_{ij} + \varepsilon$, where μ_{ij} is the mean response predicted by the dose-response model f_{ij}, and ε is the random residual which is represented as half-normal distribution $\varepsilon \sim N(0, \sigma^2)$. In the second level (i.e., the study level), we modeled the variability between studies in the hierarchical model as below:

$$a_i \sim LN(\log(\mu_a), \sigma_a), \quad \textbf{S2}$$

$$b_i \sim Unif(b_{lower}, b_{upper}), \quad \textbf{S3}$$

$$c_i \sim Unif(c_{lower}, c_{upper}), \quad \textbf{S4}$$

where the informative parameter "a" was assigned a log-normal prior distribution to ensure positive values and a realistic skewness. Note that μ_a was assumed to be a geometric mean. Regarding the non-informative parameters b and c, uniform distribution with the lower bound (b_{lower} or c_{lower}) and upper bound (b_{upper} or c_{upper}) was assigned to these parameters. The lower bound and upper bound of the non-informative parameters were determined based on the biological consideration and prior information (the prior settings will be discussed in the next section). In the third stage (i.e., the population level), the population distribution with mean μ_a and standard deviation σ_a was described as follows:

$$\mu_a \sim N(0, s_a), \quad \textbf{S5}$$

$$\sigma_a \sim Cauchy(0,\ \sigma_a), \quad \textbf{S6}$$

We used normal distribution for the location hyperparameters (i.e., μ_a) and half-Cauchy distribution for scale hyperparameters (i.e., σ_a). We put a wide variance on s_a (i.e., 1) to reflect the vague priors, while the σ_a was set a wide variance (i.e., 10) to reflect the weakly informative priors. The prior settings will be discussed in the next section.

2.1 Settings of priors for model parameters

The prior distribution is one of the critical elements in Bayesian interference. In the present study, the lognormal distribution was used in informative parameter *a*, yet the uniform distribution was used in non-informative parameters *b* and *c*. The prior settings were based on literature or prior information. For ToxCast dose-response data sets , the Hill dose-response model based on ToxCast data has been established (Watt and Judson 2018) and constrained to parameters as: (1) EC50 (parameter *a* in the present study) ranging from the minimum log(concentration) minus 2 and the maximum log(concentration), (2) Emax (parameter *b* in the present study) constrained from 0 to 1.2 (maximum response), and (3) the Hill coefficient (parameter c) constrained from 0.3 to 8. Furthermore, the Shao and Shapiro (2018) also addressed several settings in differing dose-response models for prior distributions. The current settings of model parameter priors based on the above-mention considerations are as follows:

For the 3-parameters Hill model,

$$s_a = \text{Dose}_{\text{Max}} \quad \textbf{S7}$$

$$b_{\text{lower}} = 0, \quad b_{\text{upper}} = \frac{\text{Max(Res)} - \text{Min(Res)}}{\text{Dose}_{\text{Max}} - \text{Dose}_{\text{Min}}} \times 5 \quad \textbf{S8}$$

$$c_{\text{lower}} = 0, \quad c_{\text{upper}} = 15 \quad \textbf{S9}$$

Where Max(Res) and Min(Res) are the maximum and minimum response values in the input datasets. And Dose_{Max} and Dose_{Min} are the dose levels corresponding to the maximum and

minimum responses, respectively. Based on the prior information from the previous study (Shao and Shapiro, 2018), the parameter b was defined as a slope-equivalent parameter and determined by the dose-response trend and the overall slope in the input data, which was constrained from 0 to $(\frac{\text{Max(Res)}-\text{Min(Res)}}{\text{Dose}_{\text{Max}}-\text{Dose}_{\text{Min}}} \times 5)$. On the other hand, the parameter g was constrained from 0 to 15.

For the constrained parameters of log-formed Hill model,

$$s_a = \log(\text{Dose}_{\text{Max}}) \quad \textbf{S10}$$

$$b_{\text{lower}} = 0, \quad b_{\text{upper}} = 1.2 \times \text{Max(Res)} \quad \textbf{S11}$$

$$c_{\text{lower}} = 0.3, \quad c_{\text{upper}} = 8 \quad \textbf{S12}$$

In the log-formed Hill model, the parameter b was constrained from 0 to 1.2 multiplied by the maximum response, while the parameter c was constrained from 0.3 to 8 (Watt and Judson 2018).

3. Estimation of posterior parameters

3.1. Convergence diagnosis

Four Markov chains of 10,000 iterations each, for the human, animal and ToxCast *in vitro* dose-response model, respectively, were run with the first 5,000 iterations as "burn-in" iterations and the last 5,000 iterations were used as output iterations to check convergences. Corrected Scale Reduction Factors ($\hat{R}$) were calculated for the four chains to diagnose the convergences of Markov chains based on the method of Brooks and Gelman (Brooks and Gelman, 1998). The $\hat{R}$ values of population mean (μ_a) and standard deviation (σ_a) for informative parameter "a" in the human, animal and ToxCast *in vitro* dose-response models were ≤1.05 for all simulations.

3.2. Markov chains trace plots

The Markov chains trace plots and its probability density function plots for population mean (μ_a) and standard deviation (σ_a) of the informative parameter "a" are shown in Figs. S2-S3, which

provide a visualization of the Markov chains' convergences. Specifically, a trace plot for the four chains plots the observed chain value (y-axis) against the corresponding iteration number (x-axis). The density plot for the four chains plots the observed chain value (x-axis) against density (y-axis). The well-mixed trace plots showed that the parameters reached the steady state. The trace plots of parameters *b* and *c* also reached the steady state (data not shown).

4. Estimation of human population exceedance risk

4.1. Estimation of population-based dose response analysis

At the individual level, the model predicts posterior distribution of parameters *a*, *b*, and *c* for each individual, which can be used to estimate the uncertainty for each individual's dose-response curves (Fig. 2). In the Bayesian hierarchical model (Fig. S1), population dose-response curves can be made using the estimated values of population-level parameters. In this case, the model predicts a posterior distribution for the population parameters μ_a and σ_a, from which a virtual population of *a* can be generated via Monte Carlo sampling. Because the posterior distribution of μ_a and σ_a are also sampled, two-dimensional Monte Carlo (MC) was conducted (via MCMC) to separately evaluate the variability and uncertainty in the population. First-dimension MC is to randomly sample population i = 1….5,000 from the posterior distribution of μ_a and σ_a, resulting in the distribution across i which represents the uncertainty of population mean and standard deviation. Second-dimension MC is to draw j = 1….5,000 individual pairs of $a_{i,j} \sim LN\left(\log\left(\mu_{a,i}\right), \sigma_{a,i}\right)$ based on a given set $\mu_{a,i}$ and $\sigma_{a,i}$ and non-informative parameters $b_{i,j}$ and $c_{i,j}$. The pair of each i, j indicates an individual j (variability) drawing from the population i (uncertainty). Based on the population-level parameters, the population-level dose-response curves were reconstructed based on endpoints of serum cholesterol, PPAR activation, neurotoxicity, immunotoxicity, endocrine

disruptors and cellular response, respectively.

4.2. Human biomonitoring data of the general population

To characterize the human population exceedance risk, we collected the human biomonitoring data for PFOS serum concentrations in the general population from different areas of the world and summarized in Table S2. Theses PFOS concentrations from different countries and areas were assumed lognormal distribution with the reported concentration range and treated as the probability of D in the Equation **7** to estimate the population-based risk: exceedance probability (EP). In Table S2, the observed serum PFOS concentrations range from 0.05 to 214, 3.5 to 29.6, 0.06 to 92.5, 0.4 to 1,656 ng/mL for the Asian, Australian, European, and North American populations, respectively. Median concentrations for PFOS from the North American populations appear to be higher than the European, Asian, and Australian populations (Table S2).

5. Comparison of point of departure (POD)

To better understand the results from the present Bayesian dose-response modeling, we compared the derived EC10 values from this study with the outputs from the U.S. EPA's Benchmark Dose software (BMDS) and the recently published Bayesian Benchmark Dose interface (BBMD) developed by Shao and Shapiro (2018). The BMDS and BBMD systems were used to fit the same datasets to estimate BMD doses using the default settings. To compare the EC10 values derived from this study versus the BMDS and BBMD methods, the benchmark response (BMR) was set as 10% (BMR = 0.1) in all analyses. In order to select the best-estimated BMD in the BMDS, the results of the Hill model was selected first, and then the one with the lowest Akaike information criterion (AIC) value was chosen if the Hill model failed to fit the data. For the BBMD method,

the results were selected from the model-averaged BMD based on seven different dose-response models (e.g., Linear, Power, Hill and exponential model, etc.). All the results of POD estimation from different methods across the 34 selected datasets are summarized in Table S4. The range of PODs for human studies was estimated to be 0.19–7.13, 0.27–5.96 and 6.13–19.8 ng/mL from this study, BMDS and BBMD, respectively. For animal studies, the range of PODs was estimated to 0.13–2.70 (this study), 0.11-2.14 (BMDS), and 0.31–2.57 (BBMD) mg/kg/day. In the ToxCast *in vitro* studies, the value ranged from 3.81 to 109, 0.96 to 94.23, and 0.69 to 69 μM based on the estimation of this study, BMDS and BBMD, respectively. The results showed that the PODs estimated from this study were similar to the outputs from BMDS and BBMD.

6. Supplementary Tables

Table S1

Estimated steady-state concentration (Css), area under curve (AUC), average serum concentration (ASC), and average liver concentration (ALC) in mice, rats, monkeys, and humans using a multi-species PBPK model

Species	Css (μM)	AUC_{serum} (μg/mL*h)	AUC_{liver} (μg/mL*h)	ASC (ng/mL)	ALC (ng/mL)
Mouse	-	-	6,912,827	-	462,833
Rat	-	-	1,507,243	-	172,059
Monkey	-	-	1,507,243	-	789,135
Human	13,571	41,221,651	6,325,264,367	94,113	1441,240

Note: the PBPK model simulated scenarios were daily oral exposure to PFOS at 1 mg/kg/day for 1 year in mice, rats, and monkeys, and for 50 years in humans.

Table S2
Median, minimum and maximum concentrations of PFOS in human serum of general populations from Asia, Australia, Europe and North America

PFOS Concentration (ng/mL)			n	Age (years)	Country	Reference
Median	Min	Max				
Asia						
-	≤1	3.1	45	17-48	India	Kannan et al. (2004)
7.07	1.99	26.9	150	-	Japan	Harada et al. (2010)
3.3	0.4	18.2	38	24-61	Sri Lanka	Guruge et al. (2005)
7.50	1.89	14.6	37	-	Vietnam	Harada et al. (2010)
10.23	7.28	214	1,874	19-68	Korea	Lee et al. (2017)
1.3	0.05	19	202	0-90	China	Li et al. (2017)
Australia						
20.8	12.7	29.5	40	-	Australia	Kärrman et al., (2006)
-	3.5	19.9	100	0-61+	Australia	Aylward et al. (2014)
-	5	28.5	2,420	0-60+	Australia	Toms et al. (2009)
Europe						
0.52	0.17	32	2,355	-	Sweden	Shu et al. (2018)
18.5	8.20	40.2	190	30	Poland	Lindh et al. (2012)
7.60	2.77	29.9	203	25	Ukraine	Lindh et al. (2012)
6.31	0.06	29.6	230	36-65+	Siena, Italy	Ingelido et al. (2010)
6.05	0.28	38.58	1,240	-	Spain	Matilla-Santander et al. (2017)
-	1	92.5	256	5-69	Germany	Hölzer et al. (2008)
North America						
28.4	6.7	81.5	65	-	U.S.	Hansen et al. (2001)
28.8	3.7	65.1	56	<20	Canada	Kubwabo et al. (2004)
35.8	≤4.3	1656	645	20-69	U.S.	Olsen et al. (2003)
21.1	≤0.4	435	2,094	12-60+	U.S., NHANES 2003-2004	Calafat et al. (2007)
30.2	≤3.4	175	238	65-96	Seattle, U.S.	Olsen et all. (2004b)
-	≤1.3	164	175	17-72	U.S.	Kannan et al. (2004)
36.7	6.7	515	598	2-12	U.S.	Olsen et al. (2004a)

Table S3
Posterior parameters with 95% CI at the population level

	Posterior population parameters estimation			
Type of dose-response data	$\boldsymbol{\mu_a}$	$\boldsymbol{\sigma_a}$	**b**	**c**
Human studies	16.29 (3.13 – 72.06)	39.82 (37.5 – 40.56)	39.82 (37.5 – 40.56)	0.62 (0.44 – 0.85)
Animal studies	2.53 (1.03 – 6.65)	145 (130 – 149)	145 (130 – 149)	1.65 (1.23 – 2.18)
ToxCast for PPAR activation	98.1 (33.9 – 278.7)	578 (549 – 595)	578 (549 – 595)	6.87 (4.00 – 8.89)
ToxCast for neurotoxicity	14.8 (7.0 – 32.52)	76.3 (65.6 – 93.1)	76.3 (65.6 – 93.1)	2.95 (1.37 – 7.93)
ToxCast for immunotoxicity	51.9 (27.7 – 86.8)	615 (587 – 626)	615 (587 – 626)	4.07 (3.46 – 5.68)
ToxCast for endocrine disruption	137 (58.4 – 325)	357 (315 – 365)	357 (315 – 365)	2.11 (1.53 – 3.88)
ToxCast for cellular response	189 (122 – 282)	397 (372 – 433)	397 (372 – 433)	3.65 (3.13 – 4.52)

Footnote: population mean (μ_a) and standard deviation (σ_a) of the parameter *a* reflect the variability of EC50 in the Hill dose-response model in different datasets. The unit of μ_a and σ_a is ng/mL in humans, mg/kg/day in animal studies, and μM in ToxCast *in vitro* studies. The parameter *b* with the unit of percentage (% of control change) represents the Emax in the model, and *c* represents the Hill coefficient (unitless).

Table S4

Comparison of the derived EC10 values from this study with the outputs from BMD and BBMD in the human, animal *in vivo*, and ToxCast *in vitro* studies

Reference or ToxCast assay	**This study (at EC = 0.1)**	**BMD**[a] (at BMR = 0.1)	**BBMD**[b] (at BMR = 0.1)
Human epidemiological studies			
Steenland et al. (2009)	2.28 (1.05 – 4.12)[c]	5.96 (0.94 – 10.13)	6.13 (3.44 – 8.82)
Eriksen et al. (2013)	0.19 (0.031 – 0.66)	0.27 (0.18 - 0.49)	19.8 (7.31 – 44.5)
Nelson et al. (2010)	1.85 (0.75 – 3.60)	3.99 (2.16 – 15.41)	15.45 (9.81 – 30.9)
Château-Degat et al. (2010)	7.13 (4.06 – 11.04)	4.77 (2.89 – 10.1)	9.37 (5.57 – 16.5)
Animal *in vivo* studies			
Seacat et al. (2002)	0.55 (0.32 – 1.01)	0.26 (0.15 – 0.80)	0.56 (0.22 – 1.17)
Seacat et al. (2003)	0.20 (0.12 – 0.31)	0.19 (0.12 - 0.45)	0.35 (0.13 – 0.73)
Curran et al. (2008)	2.70 (1.66 – 4.60)	0.25 (0.13 – 0.75)	2.57 (1.0 – 5.5)
Dong et al.(2009)	0.22 (0.13 – 0.33)	0.37 (0.03 – 0.39)	0.31 (0.12 – 0.63)
Dong et al. (2011)	0.13 (0.07 – 0.22)	0.11 (0.08 – 0.16)	0.75 (0.29 – 1.51)
Lefebvre et al. (2008)	2.67 (1.66 – 4.48)	2.14 (1.4 – 4.88)	2.57 (1.0 – 5.48)
ToxCast *in vitro* assays			
ATG_PPRE_CIS_up	38.1 (24.9 – 44.8)	13.99 (4.42 – 17.65)	17.11 (7.40 – 33.42)
ATG_PPARa_TRANS_up	105 (67.6 – 125)	51.06 (16.7 – 59.6)	64.15 (27.76 - 124)
ATG_PPARg_TRANS_up	16.8 (11.2 – 25.3)	19.55 (18.6 – 43.2)	69.0 (24.6 – 160.9)
NVS_GPCR_h5HT5A	3.81 (0.86 – 10.8)	3.74 (1.83 – 18.9)	12.07 (5.15 – 24.3)
NVS_GPCR_h5HT6	11.6 (3.35 – 23.8)	19.17 (18.2 – 33.11)	18.44 (8.3 – 37.8)
NVS_GPCR_h5HT7	4.04 (1.29 – 8.78)	5.29 (5.05 – 5.74)	16.2 (5.99 – 35.6)
NVS_GPCR_hAdoRA2a	1.62 (0.48 – 3.96)	5.27 (2.97 – 5.83)	9.96 (4.49 – 20.4)
NVS_GPCR_hAdra2C	6.03 (1.75 – 13.5)	16.34 (5.49 – 17.5)	5.36 (2.21 – 12.6)
NVS_GPCR_hAdrb1	9.78 (2.43 – 20.8)	18.5 (4.14 – 19.83)	9.41 (4.23 – 19.9)
BSK_SAg_CD40_down	24.4 (21.1 – 30.1)	9.64 (9.29 – 10.37)	16.1 (8.7 – 29.1)
BSK_BE3C_IP10_down	5.67 (4.77 – 6.99)	0.96 (0.76 – 1.32)	7.83 (3.43 – 47.4)
BSK_BE3C_IL1a_down	9.56 (7.91 – 14.9)	18.96 (17.29 – 21.64)	13.5 (7.9 – 39.6)
BSK_LPS_IL8_up	31.3 (25.4 – 147.6)	8.72 (3.98 – 9.91)	8.19 (2.34 – 19.9)
BSK_3C_uPAR_down	23.2 (20.1 – 28.7)	9.18 (8.88 – 9.62)	19.9 (8.98 – 40.5)
BSK_CASM3C_VCAM1_down	30.1 (24.9 – 54.8)	6.69 (4.12 – 15.24)	10.5 (2.18 – 31.1)
OT_ER_ERaERb_0480	7.76 (4.97 – 12.7)	6.54 (4.78 – 10.45)	74.5 (29.5 - 155)
ATG_ERa_TRANS_up	21.1 (14.7 – 30.8)	16.94 (16.29 – 17.86)	25.2 (10.3 – 49.3)
ATG_ERE_CIS_up	13.4 (9.6 – 20.0)	1.49 (0.83 – 3.69)	13.9 (5.39 – 28.16)
NVS_NR_hTRa_Antagonist	67.3 (39.3 – 168)	28.52 (6.26 – 87.84)	24.58 (13.37 – 46.64)
APR_HepG2_CellLoss_24h_dn	78.1 (67.8 – 90.1)	94.23 (90.9 – 99.43)	38.8 (36.4 – 41.1)
APR_HepG2_MitoMass_24h_dn	109 (94.9 – 129)	48.28 (19.22 – 86.82)	0.69 (0.11 – 61.9)
APR_HepG2_OxidativeStress_24h_up	61.7 (52.5 – 73.4)	45.55 (39.71 – 61.52)	73.3 (31.8 - 145)
APR_HepG2_p53Act_24h_up	50.2 (40.3 – 55.4)	16.54 (15.63 - 17.78)	18.3 (13.7 – 22.3)
APR_HepG2_MitoticArrest_24h_up	89.1 (77.6 – 102.2)	40.15 (31.26 – 51.19)	38.0 (32.4 – 42.1)

[a]Calculated using the EPA's Benchmark Dose Software (BMDS 3.1);

[b]Calculated using the web-based interface: Bayesian BMD (BBMD) estimation (https://benchmarkdose.org/) (Shao and Shapiro 2018);

[c]The values represent the estimated EC10 or BMD with its lower- and upper confidence limit.

7. Supplementary Figures

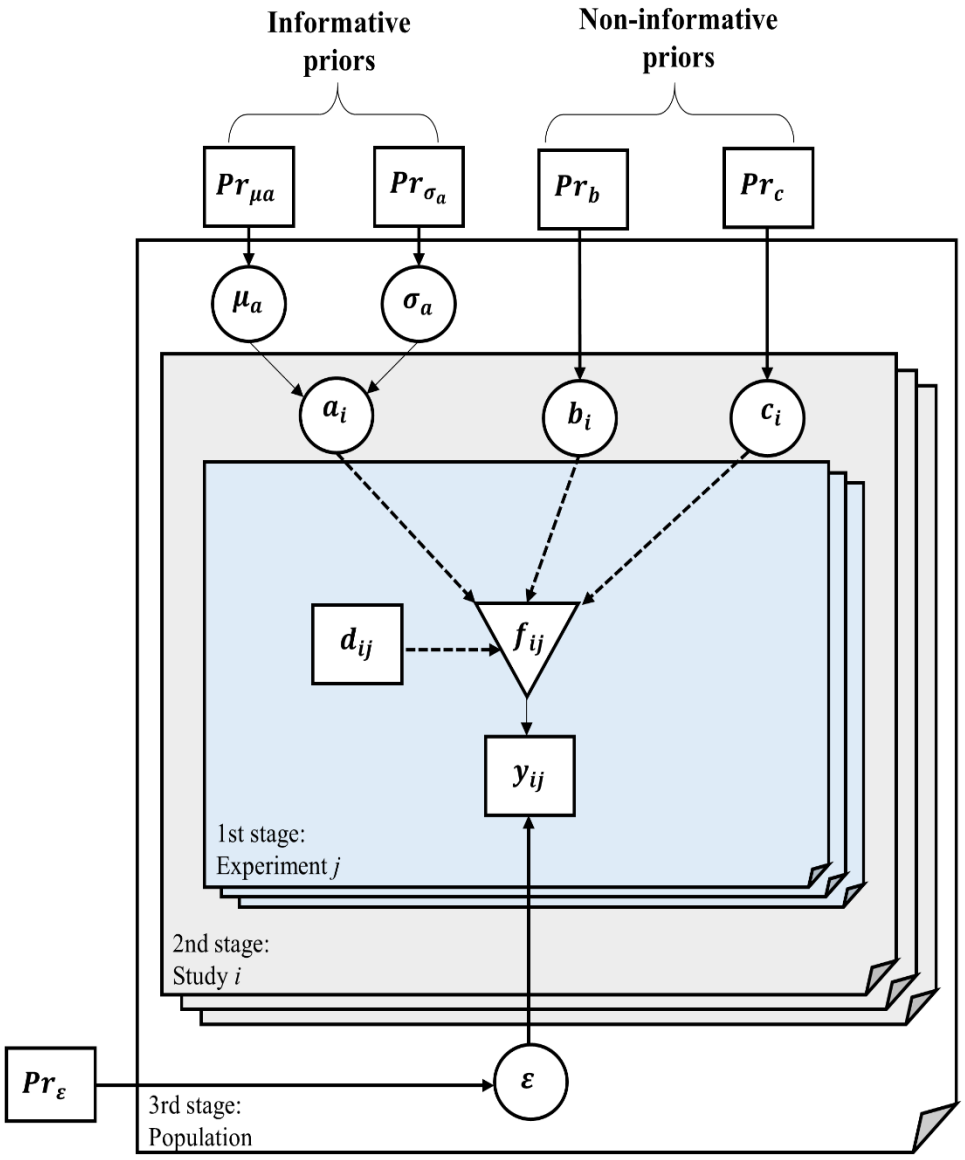

Fig. S1 Bayesian hierarchical model for the dose-response analysis (modified from Chiu et al., (2014)). The square symbol denotes a constant or an assigned probability; the circle symbol denotes a variable; and the inverted triangle symbol represents the dose-response model function. The solid arrows indicate a stochastic dependency by a conditional probability [e.g., X→Y: Y ~ P(Y|X)], while the heavy dashed arrows indicate the functional relationship [e.g., Y = f(X)]. The population consisted of studies *i*, each of which contained experiments *j*, with response data $\boldsymbol{y_{ij}}$ collected at the exposure dose $\boldsymbol{d_{ij}}$. The differences between the measured responses and predictions were assumed to have a distribution with variance $\boldsymbol{\varepsilon}$, which was assigned a prior distribution (*Pr*). The dose-response model used informative parameter $\boldsymbol{a_i}$ and non-informative parameters $\boldsymbol{b_i}$ and $\boldsymbol{c_i}$. Informative parameter $\boldsymbol{a_i}$ values were drawn from a population distribution with mean $\boldsymbol{\mu_a}$ and variance $\boldsymbol{\sigma_a}$, each of which was in turn assigned as prior distributions. Non-informative parameters were assigned the uniform distribution with lower-bound and upper-bound constrained values.

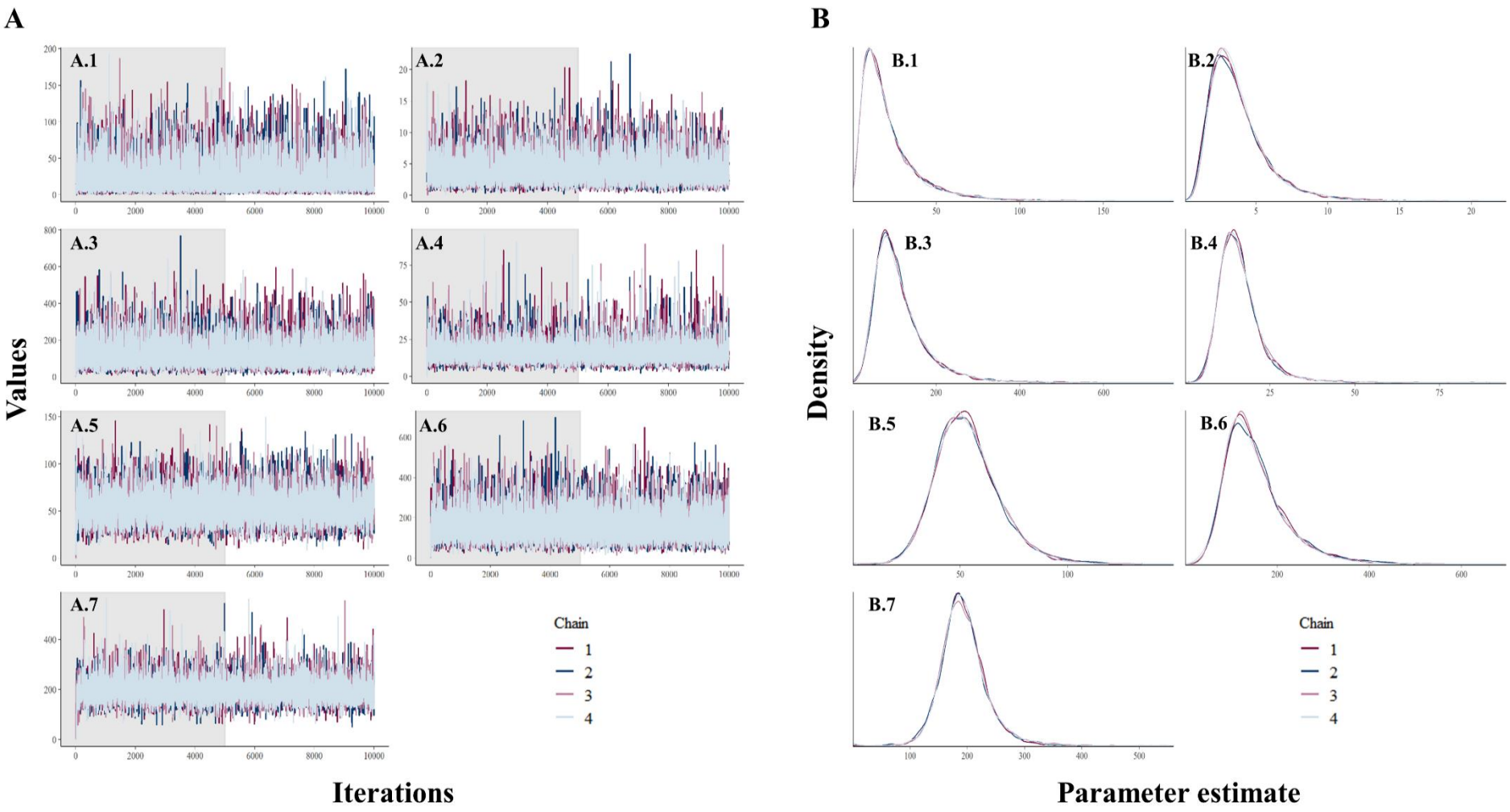

Fig. S2 Traces (A) and probability (B) density plots of four Markov chains of the last 5,000 iterations of the MCMC simulation for the population mean (μ_a) of the parameter "a" in (A1, B1) humans, (A2, B2) animals, (A3, B3) ToxCast-PPAR, (A4, B4) ToxCast-neurotoxicity, (A5, B5) ToxCast-immunotoxicity, (A6, B6) endocrine disruptors, and (A7, B7) ToxCast-cellular response. Potential scale reduction factors: $\hat{R}$ =1.0 - 1.01. Shadow area indicates the first 5,000 burn-in iterations.

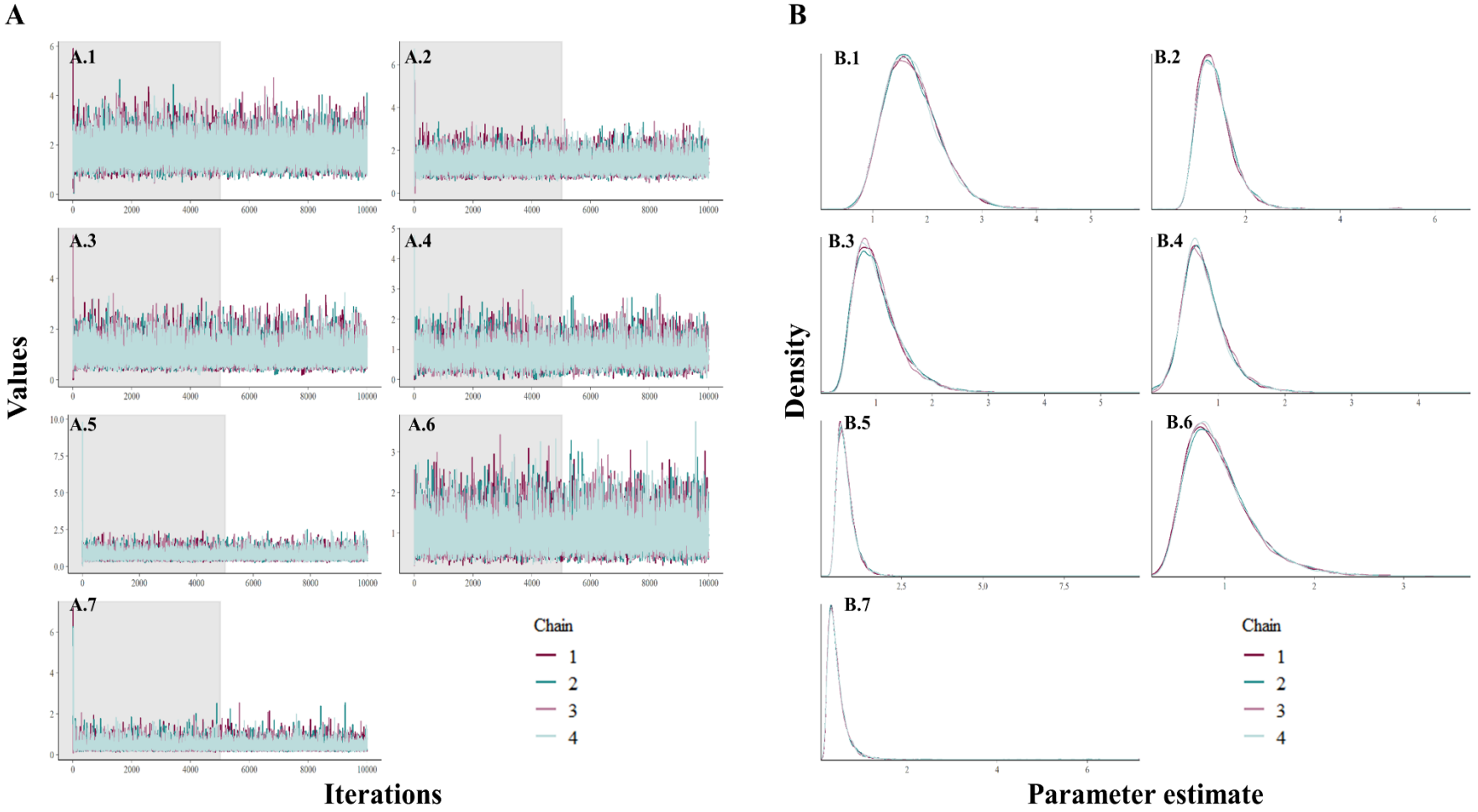

Fig. S3 Traces (A) and probability (B) density plots of four Markov chains of the last 5,000 iterations of the MCMC simulation for the population stand deviation (σ_a) of the parameter "a" in (A1, B1) humans, (A2, B2) animals, (A3, B3) ToxCast-PPAR, (A4, B4) ToxCast-neurotoxicity, (A5, B5) ToxCast-immunotoxicity, (A6, B6) endocrine disruptors, and (A7, B7) ToxCast-cellular response. Potential scale reduction factors: $\widehat{R}$ =1.0 - 1.01. Shadow area indicates the first 5,000 burn-in iterations.

8. Additional files and instructions

8.1. Additional files

The additional files include several separate zip files: **ModCode.zip**, **Datasets.zip**, **ResultsCode.zip** and **BMDS_BBMD_Analysis.zip**.

- **ModCode.zip file**: R codes for the dose-response model based on the human, animal, and ToxCast *in vitro* studies are included in this zip file.
  - STANCode: The STAN code for model fitting with the dose-response data.
  - RScript: The R code for computing the STAN code.
- **Datasets.zip file**: All datasets used in the dose-response model development are included in this zip file. Please refer to Table 1 and Table 2 for details about these datasets.
- **ResultsCode.zip file**: This zip file contains the R codes used to generate all results presented in the manuscript.

  "PlotCode" folder:
  - Code for Fig_2_3: The R code used to generate results in Fig. 2 and Fig. 3
  - Code for Fig_4: The R code used to generate results in Fig. 4.
  - Code for Fig_5: The R code used to generate results in Fig. 5 and Table 4.
  - Code for Fig_S2_S3: The R code used to generate results in Fig. S2 and Fig. S3.
  - Code for Table_3: The R code used to generate results in Table 3.

  "StanResults" folder:
  - Data.rds: The "rds" file stores all the observed data from selected human, animal and ToxCast *in vitro* studies.
  - EC10Dat.rds: This "rds" file contains the results of EC10 values estimated from the Bayesian dose-response model.

- Fit.rds: This “rds” file contains all the fitting results after running the Bayesian dose-response model. This file is not provided in this folder because the size of this file is 916 MB, which exceeds the maximum file size of 700 MB for uploading to the submission system of *Environment International*. However, this file is available upon request from the corresponding author.
- Theta.names.rds: This “rds” file stores all the parameter names used in the PBPK model.
- Snames.rds: This “rds” file stores all the parameter names used in the Bayesian dose-response model.
- MCMC_.rds: These “rds” files contain all results of the final parameter estimates from the MCMC simulations using the PBPK model in mice (MCMC_Mice.rds), rats (MCMC_Rat.rds), monkeys (MCMC_Monkey.rds), and humans (MCMC_Human.rds).
- PBPK_.rds: These “rds” files contain the PBPK-mrgsolve code for mice (PBPK_Mice.rds), rats (PBPK_Rat.rds), monkeys (PBPK_Monkey.rds), and humans (PBPK_Human.rds).

- **BMDS_BBMD_Analysis.zip file**: This zip file contains the BBMD report, BMD report and input datasets.

8.2. Instructions on the model code

- This instruction can be separated into two parts, including Part I: Dose-response model development; and Part II: reproducing all results presented in the figures and tables in the manuscript.

Part I: Dose-response model development using Stan code

- Open the supplementary files: unzip all zip files → open the folder “ModCode”→ open the R files “**STANCode**” and “**Rscript**” using RStudio.
- Set your working directory: Set your working directory as the folder “**Datasets**”.
- Run the Stan code: Run all the code in the “**STANCode**” R file to compile the dose-response model.
- Run the R code: Run the code in the “RScript” R file step by step as described below:

- Lines 1–5: Loading the required R packages
- Lines 7–11: Set up the Rstan model setting
- Lines 13 – 178: Read the datasets from external files and create a parameter list for each endpoint for use in the STAN model.
- Lines 180 – 187: Create the parameters for which you want to generate the output results
- Lines 189 – 197: Create the required parameters for running MCMC in STAN
- Lines 199 – 209: Create the list of model code and data sets
- Lines 211 – 231: Define the function for running all STAN models
- Lines 232-234: Execute the STAN model
- Lines 235-239: Create the empty list for saving the required variables of plot
- Lines 240 – 266: Execute the code for posterior dose response plots
- Lines 268 – 276: View the posterior dose-response plots
- Lines 277 – 279: Save the data and results from the STAN dose-response model simulation

Part II: Reproduce the results in the figures and tables of the manuscript

- Open the folder "ResultsCode". The folder includes two subfolders: "StanResults" and "PlotCode". The PlotCode folder stores all R codes for reproducing results presented in the figures and tables in the present manuscript. The "StanResults" folder stores the results after running the Bayesian dose-response model using STAN as different ".rds" files. Please refer to the Section 8.1 above for a detailed explanation of each ".rds" file.
- Set the working directory as the folder "StanResults" before running each figure or table code file.
- Open one of the R codes under the folder "PlotCode" and run it to reproduce the results presented in the corresponding figure and/or table in the manuscript.

9. Supplementary references

Aylward, L.L., Green, E., Porta, M., Toms, L. M., Den Hond, E., Schulz, C., Gasull, M., Pumarega, J., Conrad, A., Kolossa-Gehring, M., Schoeters, G., Mueller, J.F., 2014. Population variation in biomonitoring data for persistent organic pollutants (POPs): An examination of multiple population-based datasets for application to Australian pooled biomonitoring data. Environ. Int. 68, 127–138. https://doi.org/10.1016/J.ENVINT.2014.03.026

Brooks, S.P., Gelman, A., 1998. General Methods for Monitoring Convergence of Iterative Simulations. J. Comput. Graph. Stat. 7, 434–455. https://doi.org/10.1080/10618600.1998.10474787

Calafat, A.M., Wong, L.-Y., Kuklenyik, Z., Reidy, J.A., Needham, L.L., 2007. Polyfluoroalkyl Chemicals in the U.S. Population: Data from the National Health and Nutrition Examination Survey (NHANES) 2003–2004 and Comparisons with NHANES 1999–2000. Environ. Health Perspect. 115, 1596–1602. https://doi.org/10.1289/ehp.10598

Château-Degat, M.-L., Pereg, D., Dallaire, R., Ayotte, P., Dery, S., Dewailly, É., 2010. Effects of perfluorooctanesulfonate exposure on plasma lipid levels in the Inuit population of Nunavik (Northern Quebec). Environ. Res. 110, 710–717. https://doi.org/10.1016/J.ENVRES.2010.07.003

Chiu, W.A., Campbell, J.L., Clewell, H.J., Zhou, Y.-H., Wright, F.A., Guyton, K.Z., Rusyn, I., 2014. Physiologically Based Pharmacokinetic (PBPK) Modeling of Interstrain Variability in Trichloroethylene Metabolism in the Mouse. Environ. Health Perspect. 122, 456–463. https://doi.org/10.1289/ehp.1307623

Chen, N., Li, J., Li, D., Yang, Y., He, D., 2014. Chronic Exposure to Perfluorooctane Sulfonate Induces Behavior Defects and Neurotoxicity through Oxidative Damages, In Vivo and In Vitro. PLoS One 9, e113453. https://doi.org/10.1371/journal.pone.0113453

Chou, H.C., Wen, L.L., Chang, C.C., Lin, C.Y., Jin, L., Juan, S.H., 2017. L-carnitine via PPARγ- and Sirt1-dependent mechanisms attenuates epithelial-mesenchymal transition and renal fibrosis caused by perfluorooctanesulfonate. Toxicol. Sci. 160, 217–229. https://doi.org/10.1093/toxsci/kfx183

Curran, I., Hierlihy, S.L., Liston, V., Pantazopoulos, P., Nunnikhoven, A., Tittlemier, S., Barker, M., Trick, K., Bondy, G., 2008. Altered fatty acid homeostasis and related toxicologic sequelae in rats exposed to dietary potassium perfluorooctanesulfonate (PFOS). J. Toxicol. Environ. Heal. - Part A Curr. Issues 71, 1526–1541. https://doi.org/10.1080/15287390802361763

Das, K.P., Wood, C.R., Lin, M.J., Starkov, A.A., Lau, C., Wallace, K.B., Corton, J.C., Abbott,

B.D., 2017. Perfluoroalkyl acids-induced liver steatosis: Effects on genes controlling lipid homeostasis. Toxicology 378, 37–52. https://doi.org/10.1016/j.tox.2016.12.007

Dong, G. H., Zhang, Y. H., Zheng, L., Liu, W., Jin, Y.H., He, Q.C., 2009. Chronic effects of perfluorooctanesulfonate exposure on immunotoxicity in adult male C57BL/6 mice. Arch. Toxicol. 83, 805–815. https://doi.org/10.1007/s00204-009-0424-0

Dong, G.H., Liu, M.M., Wang, D., Zheng, L., Liang, Z.F., Jin, Y.H., 2011. Sub-chronic effect of perfluorooctanesulfonate (PFOS) on the balance of type 1 and type 2 cytokine in adult C57BL6 mice. Arch. Toxicol. https://doi.org/10.1007/s00204-011-0661-x

EFSA, 2018. Risk to human health related to the presence of perfluorooctane sulfonic acid and perfluorooctanoic acid in food, EFSA Journal. https://doi.org/10.2903/j.efsa.2018.5194

Elcombe, C.R., Elcombe, B.M., Foster, J.R., Chang, S.C., Ehresman, D.J., Butenhoff, J.L., 2012. Hepatocellular hypertrophy and cell proliferation in Sprague-Dawley rats from dietary exposure to potassium perfluorooctanesulfonate results from increased expression of xenosensor nuclear receptors PPARα and CAR/PXR. Toxicology 293, 16–29. https://doi.org/10.1016/j.tox.2011.12.014

Elcombe, C.R., Peffer, R.C., Wolf, D.C., Bailey, J., Bars, R., Bell, D., Cattley, R.C., Ferguson, S.S., Geter, D., Goetz, A., Goodman, J.I., Hester, S., Jacobs, A., Omiecinski, C.J., Schoeny, R., Xie, W., Lake, B.G., 2014. Mode of action and human relevance analysis for nuclear receptor-mediated liver toxicity: A case study with phenobarbital as a model constitutive androstane receptor (CAR) activator. Crit. Rev. Toxicol. https://doi.org/10.3109/10408444.2013.835786

Eriksen, K.T., Raaschou-Nielsen, O., McLaughlin, J.K., Lipworth, L., Tjønneland, A., Overvad, K., Sørensen, M., 2013. Association between Plasma PFOA and PFOS Levels and Total Cholesterol in a Middle-Aged Danish Population. PLoS One 8, e56969. https://doi.org/10.1371/journal.pone.0056969

Fai Tse, W.K., Li, J.W., Kwan Tse, A.C., Chan, T.F., Hin Ho, J.C., Sun Wu, R.S., Chu Wong, C.K., Lai, K.P., 2016. Fatty liver disease induced by perfluorooctane sulfonate: Novel insight from transcriptome analysis. Chemosphere 159, 166–177. https://doi.org/10.1016/j.chemosphere.2016.05.060

Fitz-Simon, N., Fletcher, T., Luster, M.I., Steenland, K., Calafat, A.M., Kato, K., Armstrong, B., 2013. Reductions in serum lipids with a 4-year decline in serum perfluorooctanoic acid and perfluorooctanesulfonic acid. Epidemiology 24, 569–576. https://doi.org/10.1097/EDE.0b013e31829443ee

Frisbee, S.J., Shankar, A., Knox, S.S., Steenland, K., Savitz, D.A., Fletcher, T., Ducatman, A.M., 2010. Perfluorooctanoic acid, perfluorooctanesulfonate, and serum lipids in children and adolescents: Results from the C8 health project. Arch. Pediatr. Adolesc. Med.

https://doi.org/10.1001/archpediatrics.2010.163

Geiger, S.D., Xiao, J., Ducatman, A., Frisbee, S., Innes, K., Shankar, A., 2014. The association between PFOA, PFOS and serum lipid levels in adolescents. Chemosphere 98, 78–83. https://doi.org/10.1016/j.chemosphere.2013.10.005

Gonzalez, F.J., Shah, Y.M., 2008. PPARα: Mechanism of species differences and hepatocarcinogenesis of peroxisome proliferators. Toxicology. https://doi.org/10.1016/j.tox.2007.09.030

Guruge, K.S., Taniyasu, S., Yamashita, N., Wijeratna, S., Mohotti, K.M., Seneviratne, H.R., Kannan, K., Yamanaka, N., Miyazaki, S., 2005. Perfluorinated organic compounds in human blood serum and seminal plasma: a study of urban and rural tea worker populations in Sri Lanka. J. Environ. Monit. 7, 371. https://doi.org/10.1039/b412532k

Han, R., Zhang, F., Wan, C., Liu, L., Zhong, Q., Ding, W., 2018. Effect of perfluorooctane sulphonate-induced Kupffer cell activation on hepatocyte proliferation through the NF-KB/TNF-A/IL-6-dependent pathway. Chemosphere 200, 283–294. https://doi.org/10.1016/j.chemosphere.2018.02.137

Harada, K.H., Yang, H.-R., Moon, C.-S., Hung, N.N., Hitomi, T., Inoue, K., Niisoe, T., Watanabe, T., Kamiyama, S., Takenaka, K., Kim, M.-Y., Watanabe, K., Takasuga, T., Koizumi, A., 2010. Levels of perfluorooctane sulfonate and perfluorooctanoic acid in female serum samples from Japan in 2008, Korea in 1994–2008 and Vietnam in 2007–2008. Chemosphere 79, 314–319. https://doi.org/10.1016/J.CHEMOSPHERE.2010.01.027

Hölzer, J., Midasch, O., Rauchfuss, K., Kraft, M., Reupert, R., Angerer, J., Kleeschulte, P., Marschall, N., Wilhelm, M., 2008. Biomonitoring of perfluorinated compounds in children and adults exposed to perfluorooctanoate-contaminated drinking water. Environ. Health Perspect. 116, 651–7. https://doi.org/10.1289/ehp.11064

Houck, K.A., Dix, D.J., Judson, R.S., Kavlock, R.J., Yang, J., Berg, E.L., 2009. Profiling Bioactivity of the ToxCast Chemical Library Using BioMAP Primary Human Cell Systems. J. Biomol. Screen. 14, 1054–1066. https://doi.org/10.1177/1087057109345525

Hu, X.-Z., Hu, D.-C., 2009. Effects of perfluorooctanoate and perfluorooctane sulfonate exposure on hepatoma Hep G2 cells. Arch. Toxicol. 83, 851–861. https://doi.org/10.1007/s00204-009-0441-z

Ingelido, A.M., Marra, V., Abballe, A., Valentini, S., Iacovella, N., Barbieri, P., Porpora, M.G., Domenico, A. di, Felip, E. De, 2010. Perfluorooctanesulfonate and perfluorooctanoic acid exposures of the Italian general population. Chemosphere 80, 1125–1130. https://doi.org/10.1016/J.CHEMOSPHERE.2010.06.025

Kärrman, A., Mueller, J.F., Van Bavel, B., Harden, F., Toms, L.M.L., Lindström, G., 2006. Levels of 12 perfluorinated chemicals in pooled Australian serum, collected 2002-2003, in relation to age, gender, and region. Environ. Sci. Technol. 40, 3742–3748. https://doi.org/10.1021/es060301u

Kleinstreuer, N.C., Dix, D.J., Houck, K.A., Kavlock, R.J., Knudsen, T.B., Martin, M.T., Paul, K.B., Reif, D.M., Crofton, K.M., Hamilton, K., Hunter, R., Shah, I., Judson, R.S., 2013. In Vitro Perturbations of Targets in Cancer Hallmark Processes Predict Rodent Chemical Carcinogenesis. Toxicol. Sci. 131, 40–55. https://doi.org/10.1093/toxsci/kfs285

Kristen J. Hansen, *, Lisa A. Clemen, Mark E. Ellefson, and, Johnson, H.O., 2001. Compound-Specific, Quantitative Characterization of Organic Fluorochemicals in Biological Matrices. https://doi.org/10.1021/ES001489Z

Kubwabo, C., Vais, N., Benoit, F.M., 2004. A pilot study on the determination of perfluorooctanesulfonate and other perfluorinated compounds in blood of Canadians. J. Environ. Monit. 6, 540. https://doi.org/10.1039/b314085g

Kannan, K., Corsolini, S., Falandysz, J., Fillmann, G., Kumar, K.S., Loganathan, B.G., et al. Perfluorooctanesulfonate and related fluorochemicals in human blood from several countries. Environ Sci Technol 2004; 38(17):4489-4495. https://doi.org/10.1021/ES0493446

Lake, B.G., 2018. Human relevance of rodent liver tumour formation by constitutive androstane receptor (CAR) activators. Toxicol. Res. (Camb). https://doi.org/10.1039/C8TX00008E

Lake, B.G., 2009. Species differences in the hepatic effects of inducers of CYP2B and CYP4A subfamily forms: Relationship to rodent liver tumour formation. Xenobiotica. https://doi.org/10.1080/00498250903098184

Lee, J.H., Lee, C.K., Suh, C.-H., Kang, H.-S., Hong, C.-P., Choi, S.-N., 2017. Serum concentrations of per- and poly-fluoroalkyl substances and factors associated with exposure in the general adult population in South Korea. Int. J. Hyg. Environ. Health 220, 1046–1054. https://doi.org/10.1016/J.IJHEH.2017.06.005

Lefebvre, D.E., Curran, I., Armstrong, C., Coady, L., Parenteau, M., Liston, V., Barker, M., Aziz, S., Rutherford, K., Bellon-Gagnon, P., Shenton, J., Mehta, R., Bondy, G., 2008. Immunomodulatory effects of dietary potassium perfluorooctane sulfonate (PFOS) exposure in adult Sprague-Dawley rats. J. Toxicol. Environ. Heal. - Part A Curr. Issues. https://doi.org/10.1080/15287390802391943

Li, Y., Cheng, Y., Xie, Z., Zeng, F., 2017. Perfluorinated alkyl substances in serum of the southern Chinese general population and potential impact on thyroid hormones. Sci.

Rep. 7, 43380. https://doi.org/10.1038/srep43380

Lin, C.Y., Wen, L.L., Lin, L.Y., Wen, T.W., Lien, G.W., Chen, C.Y., Hsu, S.H.J., Chien, K.L., Sung, F.C., Chen, P.C., Su, T.C., 2011. Associations between levels of serum perfluorinated chemicals and adiponectin in a young hypertension cohort in Taiwan. Environ. Sci. Technol. 45, 10691–10698. https://doi.org/10.1021/es201964x

Lindh, C.H., Rylander, L., Toft, G., Axmon, A., Rignell-Hydbom, A., Giwercman, A., Pedersen, H.S., Góalczyk, K., Ludwicki, J.K., Zvyezday, V., Vermeulen, R., Lenters, V., Heederik, D., Bonde, J.P., Jönsson, B.A.G., 2012. Blood serum concentrations of perfluorinated compounds in men from Greenlandic Inuit and European populations. Chemosphere 88, 1269–1275. https://doi.org/10.1016/J.CHEMOSPHERE.2012.03.049

Makela, S., Davis, V., Tally, W., Korkman, J., Salo, L., Vihko, R., Santti, R., Korach, K., 1994. Dietary Estrogens Act through Estrogen Receptor-Mediated Processes and Show No Antiestrogenicity in Cultured Breast Cancer Cells. Environ. Health Perspect. 102, 572–578. https://doi.org/10.1289/ehp.94102572

Martin, M.T., Dix, D.J., Judson, R.S., Kavlock, R.J., Reif, D.M., Richard, A.M., Rotroff, D.M., Romanov, S., Medvedev, A., Poltoratskaya, N., Gambarian, M., Moeser, M., Makarov, S.S., Houck, K.A., 2010. Impact of environmental chemicals on key transcription regulators and correlation to toxicity end points within EPA's toxcast program. Chem. Res. Toxicol. 23, 578–590. https://doi.org/10.1021/tx900325g

Matilla-Santander, N., Valvi, D., Lopez-Espinosa, M.-J., Manzano-Salgado, C.B., Ballester, F., Ibarluzea, J., Santa-Marina, L., Schettgen, T., Guxens, M., Sunyer, J., Vrijheid, M., 2017. Exposure to Perfluoroalkyl Substances and Metabolic Outcomes in Pregnant Women: Evidence from the Spanish INMA Birth Cohorts. Environ. Health Perspect. 125, 117004. https://doi.org/10.1289/EHP1062

Minata, M., Harada, K.H., Kärrman, A., Hitomi, T., Hirosawa, M., Murata, M., Gonzalez, F.J., Koizumi, A., 2010. Role of peroxisome proliferator-activated receptor-α in hepatobiliary injury induced by ammonium perfluorooctanoate in mouse liver. Ind. Health 48, 96–107. https://doi.org/10.2486/indhealth.48.96

Montgomery, R., T.W. Conway, and A.A. Spector. 1990. Biochemistry: A Case-Oriented Approach. 5th ed. The C.V. Mosby Company, St. Louis, MO.

Nelson, J.W., Hatch, E.E., Webster, T.F., 2010. Exposure to polyfluoroalkyl chemicals and cholesterol, body weight, and insulin resistance in the general U.S. population. Environ. Health Perspect. https://doi.org/10.1289/ehp.0901165

Olsen, G.W., Church, T.R., Hansen, K.J., Burris, J.M., Butenhoff, J.L., Mandel, J.H., Zobel, L.R., 2004a. Quantitative Evaluation of Perfluorooctanesulfonate (PFOS) and Other Fluorochemicals in the Serum of Children. J. Child. Heal. 2, 53–76.

https://doi.org/10.3109/15417060490447378

Olsen, G.W., Church, T.R., Larson, E.B., van Belle, G., Lundberg, J.K., Hansen, K.J., Burris, J.M., Mandel, J.H., Zobel, L.R., 2004b. Serum concentrations of perfluorooctanesulfonate and other fluorochemicals in an elderly population from Seattle, Washington. Chemosphere 54, 1599–1611. https://doi.org/10.1016/j.chemosphere.2003.09.025

Olsen, G.W., Church, T.R., Miller, J.P., Burris, J.M., Hansen, K.J., Lundberg, J.K., Armitage, J.B., Herron, R.M., Medhdizadehkashi, Z., Nobiletti, J.B., O'Neill, E.M., Mandel, J.H., Zobel, L.R., 2003. Perfluorooctanesulfonate and other fluorochemicals in the serum of American Red Cross adult blood donors. Environ. Health Perspect. 111, 1892–1901. https://doi.org/10.1289/ehp.6316

Palmer, C.N., Hsu, M.H., Griffin, K.J., Raucy, J.L., Johnson, E.F., 1998. Peroxisome proliferator activated receptor-alpha expression in human liver. Mol. Pharmacol. 53, 14–22. https://doi.org/10.1124/mol.53.1.14

Palmisano, B.T., Zhu, L., Stafford, J.M., 2017. Role of estrogens in the regulation of liver lipid metabolism, in: Advances in Experimental Medicine and Biology. Springer New York LLC, pp. 227–256. https://doi.org/10.1007/978-3-319-70178-3_12

Pierozan, P., Karlsson, O., 2018. PFOS induces proliferation, cell-cycle progression, and malignant phenotype in human breast epithelial cells. Arch. Toxicol. 92, 705–716. https://doi.org/10.1007/s00204-017-2077-8

Seacat, A.M., Thomford, P.J., Hansen, K.J., Clemen, L.A., Eldridge, S.R., Elcombe, C.R., Butenhoff, J.L., 2003. Sub-chronic dietary toxicity of potassium perfluorooctanesulfonate in rats. Toxicology. https://doi.org/10.1016/S0300-483X(02)00511-5

Seacat, A.M., Thomford, P.J., Hansen, K.J., Olsen, G.W., Case, M.T., Butenhoff, J.L., 2002. Subchronic toxicity studies on perfluorooctanesulfonate potassium salt in cynomolgus monkeys. Toxicol. Sci. 68, 249–264. https://doi.org/10.1093/toxsci/68.1.249

Shah, I., Woodrow Setzer, R., Jack, J., Houck, K.A., Judson, R.S., Knudsen, T.B., Liu, J., Martin, M.T., Reif, D.M., Richard, A.M., Thomas, R.S., Crofton, K.M., Dix, D.J., Kavlock, R.J., 2016. Using toxcastTM data to reconstruct dynamic cell state trajectories and estimate toxicological points of departure. Environ. Health Perspect. 124, 910–919. https://doi.org/10.1289/ehp.1409029

Shao, K., Shapiro, A.J., 2018. A Web-Based System for Bayesian Benchmark Dose Estimation. Environ. Health Perspect. 126, 017002. https://doi.org/10.1289/EHP1289

Shipley, J.M., Hurst, C.H., Tanaka, S.S., DeRoos, F.L., Butenhoff, J.L., Seacat, A.M., Waxman, D.J., 2004. trans-Activation of PPAR and Induction of PPAR Target Genes by

Perfluorooctane-Based Chemicals. Toxicol. Sci. 80, 151–160. https://doi.org/10.1093/toxsci/kfh130

Shizu, R., Benoki, S., Numakura, Y., Kodama, S., Miyata, M., Yamazoe, Y., Yoshinari, K., 2013. Xenobiotic-Induced Hepatocyte Proliferation Associated with Constitutive Active/Androstane Receptor (CAR) or Peroxisome Proliferator-Activated Receptor α (PPARα) Is Enhanced by Pregnane X Receptor (PXR) Activation in Mice. PLoS One 8, e61802. https://doi.org/10.1371/journal.pone.0061802

Shu, H., Lindh, C.H., Wikström, S., Bornehag, C.-G., 2018. Temporal trends and predictors of perfluoroalkyl substances serum levels in Swedish pregnant women in the SELMA study. PLoS One 13, e0209255. https://doi.org/10.1371/journal.pone.0209255

Sipes, N.S., Martin, M.T., Kothiya, P., Reif, D.M., Judson, R.S., Richard, A.M., Houck, K.A., Dix, D.J., Kavlock, R.J., Knudsen, T.B., 2013. Profiling 976 ToxCast chemicals across 331 enzymatic and receptor signaling assays. Chem. Res. Toxicol. 26, 878–895. https://doi.org/10.1021/tx400021f

Skuladottir, M., Ramel, A., Rytter, D., Haug, L.S., Sabaredzovic, A., Bech, B.H., Henriksen, T.B., Olsen, S.F., Halldorsson, T.I., 2015. Examining confounding by diet in the association between perfluoroalkyl acids and serum cholesterol in pregnancy. Environ. Res. 143, 33–38. https://doi.org/10.1016/j.envres.2015.09.001

Slotkin, T.A., MacKillop, E.A., Melnick, R.L., Thayer, K.A., Seidler, F.J., 2008. Developmental Neurotoxicity of Perfluorinated Chemicals Modeled in Vitro. Environ. Health Perspect. 116, 716–722. https://doi.org/10.1289/ehp.11253

Starling, A.P., Engel, S.M., Whitworth, K.W., Richardson, D.B., Stuebe, A.M., Daniels, J.L., Haug, L.S., Eggesbø, M., Becher, G., Sabaredzovic, A., Thomsen, C., Wilson, R.E., Travlos, G.S., Hoppin, J.A., Baird, D.D., Longnecker, M.P., 2014. Perfluoroalkyl substances and lipid concentrations in plasma during pregnancy among women in the Norwegian Mother and Child Cohort Study. Environ. Int. 62, 104–112. https://doi.org/10.1016/j.envint.2013.10.004

Steenland, K., Tinker, S., Frisbee, S., Ducatman, A., Vaccarino, V., 2009. Association of Perfluorooctanoic Acid and Perfluorooctane Sulfonate With Serum Lipids Among Adults Living Near a Chemical Plant. Am. J. Epidemiol. 170, 1268–1278. https://doi.org/10.1093/aje/kwp279

Steenland, Kyle, Tinker, S., Frisbee, S., Ducatman, A., Vaccarino, V., 2009. Association of perfluorooctanoic acid and perfluorooctane sulfonate with serum lipids among adults living near a chemical plant. Am. J. Epidemiol. 170, 1268–1278. https://doi.org/10.1093/aje/kwp279

Takacs, M.L., Abbott, B.D., 2007. Activation of mouse and human peroxisome proliferator-

activated receptors (α, β/δ, γ) by perfluorooctanoic acid and perfluorooctane sulfonate. Toxicol. Sci. 95, 108–117. https://doi.org/10.1093/toxsci/kfl135

Toms, L.-M.L., Calafat, A.M., Kato, K., Thompson, J., Harden, F., Hobson, P., Sjödin, A., Mueller, J.F., 2009. Polyfluoroalkyl Chemicals in Pooled Blood Serum from Infants, Children, and Adults in Australia. Environ. Sci. Technol. 43, 4194–4199. https://doi.org/10.1021/es900272u

U.S. EPA, 2016. Health Effects Support Document for for Perfluorooctane Sulfonate (PFOS). EPA 822-R-16-002. Washington, D.C., U.S. Environmental Protection Agency. Available: https://www.epa.gov/sites/production/files/2016-05/documents/pfos_hesd_final_508.pdf [accessed 1 August 2019].

Vanden Heuvel, J.P., Thompson, J.T., Frame, S.R.S.R., Gillies, P.J., 2006. Differential activation of nuclear receptors by perfluorinated fatty acid analogs and natural fatty acids: A comparison of human, mouse, and rat peroxisome proliferator-activated receptor-α, -β, and -γ, liver X receptor-β, and retinoid X receptor-α. Toxicol. Sci. 92, 476–489. https://doi.org/10.1093/toxsci/kfl014

Wambaugh, J.F., Setzer, R.W., Pitruzzello, A.M., Liu, J., Reif, D.M., Kleinstreuer, N.C., Wang, N.C.Y., Sipes, N., Martin, M., Das, K., DeWitt, J.C., Strynar, M., Judson, R., Houck, K.A., Lau, C., 2013. Dosimetric anchoring of In vivo and In vitro studies for perfluorooctanoate and perfluorooctanesulfonate. Toxicol. Sci. https://doi.org/10.1093/toxsci/kft204

Wan, C., Han, R., Liu, L., Zhang, F., Li, F., Xiang, M., Ding, W., 2016. Role of miR-155 in fluorooctane sulfonate-induced oxidative hepatic damage via the Nrf2-dependent pathway. Toxicol. Appl. Pharmacol. 295, 85–93. https://doi.org/10.1016/j.taap.2016.01.023

Wang, Y., Starling, A.P., Haug, L.S., Eggesbo, M., Becher, G., Thomsen, C., Travlos, G., King, D., Hoppin, J.A., Rogan, W.J., Longnecker, M.P., 2013. Association between Perfluoroalkyl substances and thyroid stimulating hormone among pregnant women: a cross-sectional study. Environ. Heal. 12, 76. https://doi.org/10.1186/1476-069X-12-76

Watt, E.D., Judson, R.S., 2018. Uncertainty quantification in ToxCast high throughput screening. PLoS One 13, e0196963. https://doi.org/10.1371/journal.pone.0196963

Xu, C., Jiang, Z.Y., Liu, Q., Liu, H., Gu, A., 2017. Estrogen receptor beta mediates hepatotoxicity induced by perfluorooctane sulfonate in mouse. Environ. Sci. Pollut. Res. 24, 13414–13423. https://doi.org/10.1007/s11356-017-8943-3

Yu, Z., Zhang, L., Wu, D., Liu, F., 2005. Anti-apoptotic action of zearalenone in MCF-7 cells. Ecotoxicol. Environ. Saf. 62, 441–446. https://doi.org/10.1016/j.ecoenv.2004.10.003

Zeng, Z., Song, B., Xiao, R., Zeng, G., Gong, J., Chen, M., Xu, P., Zhang, P., Shen, M., Yi,

H., 2019. Assessing the human health risks of perfluorooctane sulfonate by in vivo and in vitro studies. Environ. Int. 126, 598–610. https://doi.org/10.1016/J.ENVINT.2019.03.002